Biomaterials 35 (2014) 2952–2960

Contents lists available at ScienceDirect

Biomaterials

journal homepage: www.elsevier.com/locate/biomaterials

Tumor cell membrane-targeting pH-dependent electron donor-acceptor fluorescence systems with low background signals

Liang Han [a,b], Mingming Liu [c], Deyong Ye [c], Ning Zhang [d], Ed Lim [d], Jing Lu [d], Chen Jiang [a,b,*]

[a] Key Laboratory of Molecular Engineering of Polymers of Ministry of Education, Fudan University, Shanghai 201203, China
[b] Department of Pharmaceutics, School of Pharmacy, Fudan University, Shanghai 201203, China
[c] Department of Medical Chemistry, School of Pharmacy, Fudan University, Shanghai 201203, China
[d] In Vivo Imaging R&D, Caliper Life Sciences, A Perkin Elmer Company, Alameda, CA 94501, USA

ARTICLE INFO

Article history:
Received 16 October 2013
Accepted 11 December 2013
Available online 2 January 2014

Keywords:
Dopamine
Electron donor-acceptor
Fluorescence system
pH-dependent
Tumor cell membrane targeting delivery

ABSTRACT

Minimizing the background signal is crucial for developing tumor-imaging techniques with sufficient specificity and sensitivity. Here we use pH difference between healthy tissues and tumor and tumor targeting delivery to achieve this goal. We synthesize fluorophore-dopamine conjugate as pH-dependent electron donor-acceptor fluorescence system. Fluorophores are highly sensitive to electron-transfer processes, which can alter their optical properties. The intrinsic redox properties of dopamine are oxidation of hydroquinone to quinone at basic pH and reduction of quinone to hydroquinone at acidic pH. Quinone can accept electron then quench fluorescence. We design tumor cell membrane-targeting carrier for delivery. We demonstrate quenched fluorophore-quinone can be specially transferred to tumor extracellular environment and tumor-accumulated fluorophore can be activated by acidic pH. These tumor-targeting pH-dependent electron donor-acceptor fluorescence systems may offer new opportunity for developing tumor-imaging techniques.

1. Introduction

In recent years, high-sensitivity fluorescence imaging has been increasingly investigated as a powerful research tool [1,2]. The technological advances have led numerous research groups to focus their attention on the development of non-invasive in vivo fluorescence imaging applications [3,4]. Particular attention has been put on tumor specific fluorescence imaging for early diagnosis [5]. However, extremely few fluorescence-imaging systems have been demonstrated efficient in detecting early tumor due to the high interferential signal [6,7]. Hence, to design and construct remarkably specific and sensitive fluorescence imaging systems becomes an urgent matter.

A unique aspect of optical imaging is that fluorescence probes can be designed to be sensitive, i.e. only turned on under certain conditions. The sensitive strategy is recently emerging as an attractive modality and has attracted great interest. These probes can be designed to emit signal only after binding a target tissue, greatly increasing sensitivity and specificity in the detection of disease. There are two basic types of activatable fluorescence probes [8–10]. The first kind is conventional enzymatically activatable probes. This kind exists in the quenched state until activated by enzymatic cleavage mostly outside of the cells. The second kind is newly designed target-cell specific activatable probes. This kind of probes is quenched until activated in targeted cells by endolysosomal processing [11]. However, enzyme activation typically occurs in the extracellular environment permitting diffusion away from the target cell [11]. The target-cell specific activatable probes still leads to strong background signal due to the non-tumor-specific binding on the targeting sites (ex. receptors) at normal cells [12]. Current tumor intracellular targeting strategies are mainly based on many receptors over-expressed on the surface of tumor cells and receptor-mediated endocytosis. However, these tumor targets (receptors) are not uniquely expressed in cancer cells but also in certain healthy cells, leading to unwanted background signal [13–16]. Therefore, it is important to ask whether other, more feasible, strategies might be exploited for regulating the fluorescence intensity on the basis of association with the pathological and physiological differences between tumor and normal tissues [17–19].

Boron-chelated tetraarylazadipyrromethenes are a class of red/near-infrared fluorophores [20,21]. These fluorophores can be relatively easily synthesized and amenable to structural

* Corresponding author. Department of Pharmaceutics, School of Pharmacy, Fudan University, 826 Zhangheng Road, Shanghai 201203, China. Tel./fax: +86 21 51980079.
E-mail address: jiangchen@shmu.edu.cn (C. Jiang).

0142-9612/$ – see front matter © 2014 Elsevier Ltd. All rights reserved.
http://dx.doi.org/10.1016/j.biomaterials.2013.12.020

modification. They exhibit excellent spectral properties, such as high extinction coefficients (70 000–80 000 M^{-1} cm^{-1}), high fluorescence quantum yields above 700 nm and excellent sensitivity to electron-transfer process [22]. Recently, the monoalkyne-monophenol-substituted boron-chelated tetraarylazadipyrromethene (compound **2**) has been synthesized as pH-responsive fluorophore [23]. The intensity of fluorescence output is controlled by a phenol/phenolate interconversion based on the electron transfer. Besides, the covalent attachment of fluorophore to electron acceptor can also quench the fluorescence by electron transfer [24–26]. Dopamine, a FDA-approved small-molecule drug, can be used for designing electron donor-acceptor systems [24–26]. The intrinsic redox properties of dopamine are oxidation of hydroquinone to quinone at basic pH and reduction of quinone to hydroquinone at acidic pH. Quinone can accept electron then quench fluorescence. The pathological features of tumors including acidity can be employed to change the electron transfer between the fluorophore and acceptors *via* changing the structure of the electron acceptor. Thus different fluorescence behavior would be shown in tumor environments and normal environments. Electron transfer can be utilized to activate/quench the fluorescence emission.

Herein, we show that low interferential signal could be accomplished through regulating the electron transfer by pH. Acidity (pH 6.0–6.8) is a property of tumor extracellular environments [27–29]. This characteristic is pervasive in almost all solid tumors and can be easily accessed. Acidosis is associated with tumor development both at the early stage and the advanced stage [30,31]. Our idea is realized by the covalent conjugation of boron-chelated tetraarylazadipyrromethenes with dopamine (**9A**, Fig. 1). We designed tumor cell membrane-targeting carrier for delivery. pH (low) insertion peptide (pHLIP) was utilized as the tumor cell membrane-targeting ligand. pHLIP is a water-soluble peptide derived from the transmembrane (TM) helix C of bacteriorhodopsin

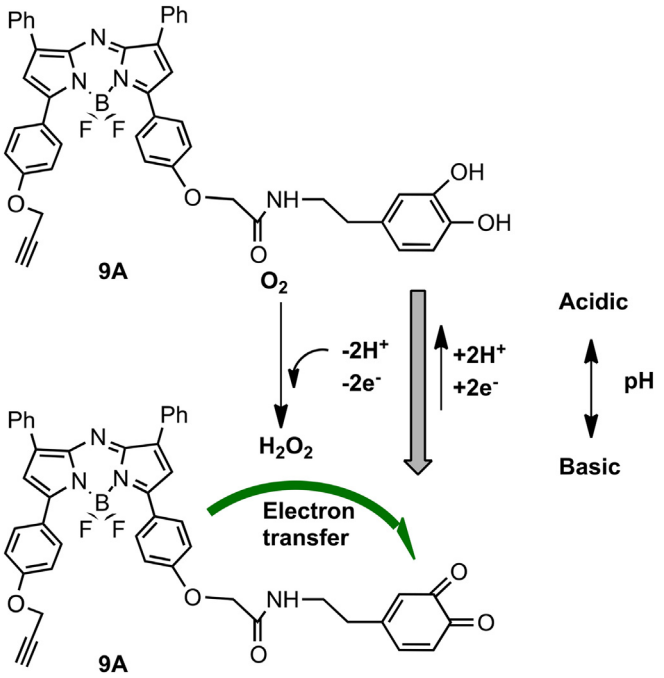

Fig. 1. pH-dependent electron donor-acceptor fluorescence system **9A**. The intrinsic redox properties of dopamine are oxidation of hydroquinone to quinone at basic pH and reduction of quinone to hydroquinone at acidic pH. Quinone can accept electron then quench fluorescence. Through the covalent conjugation of boron-chelated tetraarylazadipyrromethenes with dopamine, the electron transfer is mediated by pH.

[32]. At pH values above seven, pHLIP in solution partitions to the surface of a lipid bilayer without inserting, and at a slightly acidic pH it inserts with a pKa of ~6 in vitro to form a TM helix [32]. Nano systems exhibit many advantages over small-molecule formulations, including targeted delivery, diminished systemic toxicity and improved circulation time. [33] Improved circulation time can make sufficient contact with alkalescent physiological environment for complete quenching of fluorescence and low interferential signal. Thus nanoscale Dendri-graft poly-L-lysines (DGL, Generation 2 with 48 amino groups per molecular) were utilized as the basic carrier. We finally constructed the tumor extracellular environment targeting pH-dependent activatable imaging systems **DPP-2** and **DPP-9A**. The targeting and imaging capability of **DPP-2** and **DPP-9A** in liver tumor, breast cancer and brain tumor were evaluated in vitro and in vivo.

2. Materials and methods

2.1. Synthesis of fluorophore *9A*

The synthetic procedure is illustrated in Supplementary Information, Fig. S1. Briefly, a 1 g quantity (5.79 mmol) of 3-hydroxytyramine hydrochloride (dopamine-salt, compound **3**, Aldrich) was dispersed in methanol. Following addition of chloroacetyl chloride (0.48 mL, 6.37 mmol) and diisopropylethylamine (1.11 mL, 6.37 mmol), the reaction mixture was stirred for 2 h under ice water bath to get compound **4**. Then compound **4** (1.33 g, 5.79 mmol) was dissolved in dry CH_2Cl_2 (30 mL), treated with chloromethyl methyl ether (1.17 g, 14.53 mmol) and diisopropylethylamine (3.03 mL, 17.33 mmol), and stirred to obtain compound **5**. A solution of fluorophore **2** (200 mg, 352.48 μmol) in methyl cyanide (15 mL) was treated with K_2CO_3 (146 mg, 1.06 mmol), compound **5** (167 mg, 528.72 μmol) and tetrabutylammonium iodide, and heated under reflux for 24 h. Purification by column chromatography on silica eluting with Hexane/EtOAc (1:1) gave the MOMCl-protected **8A**. An 8 mg quantity of MOMCl-protected **8A** was dissolved in 2 mL of THF. A 0.2 mL aliquot of 9 mmol/L HCl/THF (1:2, v:v) was slowly added, and the reaction mixture was stirred overnight at room temperature. Water was added, and the resulting suspension extracted with EtOAc. The combined organic phases were evaporated to dryness, washed with Hexane and filtered to give the fluorophore **9A**. Compound **4**: ^{1}H NMR (400 MHz, $CDCl_3$, δ): 9.66 (s, 1H), 6.76–6.59 (m, 3H), 5.63 (s, 1H), 5.13 (s, 1H), 4.01 (s, 2H), 3.67 (t, J = 5.1 Hz, 1H), 3.39 (t, J = 5.0 Hz, 1H), 2.65 (tt, J = 5.1, 1.1 Hz, 2H). ^{13}C NMR ($CDCl_3$, δ): 166.68, 145.44, 144.77, 132.51, 120.30, 116.20, 115.92, 43.17, 40.59, 39.04. Compound **5**: ^{1}H NMR (400 MHz, $CDCl_3$): δ 7.11(d, J = 8.4 Hz, 1H), 7.01 (s, 1H), 6.80(d, J = 8.4 Hz, 1H), 6.62 (brs, 1H), 5.23 (d, J = 1.2 Hz, 2H), 5.22 (d, J = 1.2 Hz, 2H), 4.04 (s, 2H), 3.52–3.56(m, 8H), 2.78 (t, J = 7.6 Hz, 2H). ^{13}C NMR ($CDCl_3$, δ): 166.68, 147.05, 145.50, 132.12, 121.24, 117.25, 116.65, 95.30, 94.63, 56.45, 43.17, 40.59, 39.04. Compound **8A**: ^{1}H NMR (400 MHz, $CDCl_3$, δ): 9.06 (s, 1H), 7.65–7.57 (m, 2H), 7.55–7.30 (m, 10H), 7.22 (dt, J = 7.3, 1.6 Hz, 2H), 7.11–6.98 (m, 4H), 6.86–6.76 (m, 2H), 6.68 (ddt, J = 7.5, 2.1, 1.0 Hz, 1H), 6.40 (s, 1H), 6.02 (s, 4H), 5.60 (s, 1H), 4.68 (d, J = 2.9 Hz, 2H), 4.45 (s, 2H), 3.41–3.33 (m, 3H), 2.65 (tt, J = 5.7, 1.0 Hz, 2H). ^{13}C NMR ($CDCl_3$, δ): 170.45, 170.38, 170.32, 169.13, 160.76, 158.67, 158.64, 158.57, 158.50, 157.12, 157.06, 156.99, 149.08, 149.01, 148.95, 147.10, 145.50, 134.56, 132.15, 132.11, 129.76, 128.84, 128.82, 128.73, 128.57, 128.48, 128.09, 127.75, 123.94, 123.82, 122.77, 121.24, 117.24, 116.66, 115.70, 115.13, 95.30, 94.63, 91.66, 78.69, 76.15, 68.09, 56.45, 56.22, 40.59, 38.93. Compound **9A**: [red metallic solid] ^{1}H NMR (400 MHz, acetone-d_6): δ 8.22–8.27(m, 8H), 7.47–7.58(m, 9H), 7.19(d, 2H, J = 8.8 Hz, 2H), 7.12(d, J = 8.8 Hz, 2H), 6.74–6.76 (m, 2H), 6.54–6.57 (m, 1H), 4.96(d, J = 2.4 Hz, 2H), 4.62 (s, 2H), 3.44–3.49(m, 2H), 3.20(t, J = 2.4 Hz, 1H), 2.70(t, J = 2.4 Hz, 1H). ^{13}C NMR ($CDCl_3$, δ): 170.45, 170.38, 170.32, 169.13, 160.76, 158.67, 158.64, 158.57, 158.50, 157.12, 157.06, 156.99, 149.08, 149.01, 148.95, 145.44, 144.77, 134.56, 132.55, 132.11, 129.76, 128.84, 128.82, 128.73, 128.57, 128.48, 128.09, 127.75, 123.94, 123.82, 122.77, 120.30, 116.20, 115.92, 115.70, 115.13, 91.66, 78.69, 76.15, 68.09, 56.22, 40.59, 38.93. EI-MS (m/z): 760.8 $[M]^+$.

2.2. Preparation of micelle for *2*, *7* and *9A*

For in vitro characterization, free fluorophores needs to be encapsulated in micelle for further treatment. Compound **2**, **7**, and **9A** (0.005 mmol) were dissolved in THF (1 mL) and Cremophor EL (0.1 mL) added, respectively. The mixture was sonicated for 30 min followed by removal of the THF under reduced pressure. The resulting blue oil was dissolved in 25 mL of saline solution and filtered through an Acrodisc 25 mm syringe filter (with 0.2 μm HT Tuffryn membrane). Final concentration was checked by UV-visible spectral analysis.

2.3. Fluorescence spectral profiles

PBS in pH 4.0–9.0 was added to the solution of **7**, **2**, and **9A** in DMSO (20 μg Boron-chelated tetraarylazadipyrromethenes Unit/ml) with the volume ratio at 1:1 and the mix was incubated for 12 h and then the fluorescence was monitored at excitation 640 nm and emission was recorded in the interval of 650–800 nm

(1.5 mm slit) on a Perkin–Elmer LS-55 spectrofluorometer. Fluorescence pH spectra were also imaged by Cri imaging system (CRi, MA, USA).

2.4. Bel-7402 tumor cell culture

Human hepatocellular carcinoma cells (Bel-7402) were purchased from Cell Bank, Chinese Academy of Sciences (Shanghai, China). Briefly, Bel-7402 were maintained in RPMI Medium 1640 (Invitrogen Corporation) supplemented with 10% heat-inactivated fetal calf serum (FCS), 100 U/ml penicillin, and 100 μg/ml streptomycin and cultured at 37 °C under a humidified atmosphere containing 5% CO_2.

2.5. Cellular uptake of free fluorophores

Bel-7402 cells seeded onto a 24-well chambered glass slide and allowed to attach for 24 h. The media was then replaced with 200 μL of micelle of **7**, **2**, or **9A** (5 μg fluorophore unit/ml) and incubated for 30 min. Cells were also stained with lysotracker green to label acidic organelles. Cells were then washed once with PBS and examined by fluorescence microscope.

2.6. Synthesis of tumor cell membrane-targeting fluorophore

DGL (860 μg, 0.1 μmol) was reacted with MAL-PEG3500-NHS (1.4 mg, 0.4 μmol) at a 1:4 molar ratio in PBS (pH 8.0, 110 μL) for 2 h at room temperature. The primary amino groups on the surface of DGL were specifically reacted with the terminal NHS groups of the bifunctional PEG derivative at pH 8.0 to give DGL-PEG. Then DGL-PEG was reacted with cys-pHLIP (0.82 mg, 0.2 μmol, 5 mg mL^{-1} in DMF) at a 1:2 molar ratio in 328 μL of pH 7.0 phosphate buffered solution/DMSO (3:1, v/v) at room temperature for 24 h to form DGL-PEG-pHLIP (**DPP**). Then **DPP** was reacted with N_3-PEG2000-NHS (10 mg, 5 μmol) at a 1:50 molar ratio in PBS (pH 8.0, 1 mL) for 2 h at room temperature. The conjugates were purified by centrifugation for 12 000 rpm × 30 min × 3 times at 4 °C *via* an Amicon Ultra-4 and -15 Centrifugal Filter Units (Millipore) through Ultracel regenerated cellulose membrane (cut-off = 10 kDa). A solution of 2 (0.12 g, 0.21 mmol), 7 (127.3 mg, 0.21 mmol) or 9A (159.7 mg, 0.21 mmol) in THF:H_2O (15 mL, 3:1) was treated with a H_2O (15 mL, 3:1) solution of **DPP** (10.5 μmol), Cu(0) (13 mg, 0.21 mmol), $CuSO_4.5H_2O$ (7 mg, 0.042 mmol) and Na-ascorbate (21 mg, 0.1 mmol). The reaction mixture was heated at reflux for 3 h under N_2, cooled to RT and partitioned between EtOAc (25 mL) and water (25 mL). The combined water layers were dried and gave the imaging systems **DPP-2**, **DPP-7** and **DPP-9A**.

2.7. Fluorescence spectral profiles of *DPP-7*, *DPP-2*, and *DPP-9A*

The PBS (450 μL) in pH 4.0–9.0 and DMSO (450 μL) was added to the solution (100 μL) of **DPP-7**, **DPP-2**, and **DPP-9A** in DMSO (100 μg Boron-chelated tetraarylazadipyrromethenes Unit/ml) and the mix was incubated for 12 h and then the fluorescence was monitored at excitation 640 nm and emission was recorded in the interval of 650–800 nm (1.5 mm slit) on a Perkin–Elmer LS-55 spectrofluorometer.

2.8. Confocal imaging at different pH

Bel-7402 tumor cells were first stained with Wheat Germ Agglutinin-Alexa Fluor® 350 (5 μg/ml) for 10 min and then treated with **DPP-9A**, or **DPP-7** (5 μg fluorophore unit/ml) in medium 6.5. The 33-mm glass dish was placed firmly under confocal microscope. Images were taken 1) after 5 min incubation; 2) after the medium 6.5 was replaced by medium 7.4; 3) after the medium was replaced by medium 6.5; and 4) the medium 6.5 was removed and cells were washed three times by PBS 7.4 and replaced by medium 6.5. The fluorescent microscope settings were set (and used unchanged throughout the experiment) with the cell membrane staining (Wheat Germ Agglutinin-Alexa Fluor® 350) used to determine the cell integrity and the plane focus.

2.9. Glioma cell culture

U87MG were obtained from American Type Culture Collection (ATCC) and cultured at 37 °C in a humidified 5% CO_2 atmosphere. Growth medium was supplemented with fetal bovine serum (FBS) (10% v/v), streptomycin (100 mg/ml) and penicillin (100 units/ml). All cells were grown as monolayers in 75 cm^2 culture flasks and were harvested when they reached 80% confluence to maintain exponential growth.

2.10. Fluorescence microscope imaging at different pH

U87 glioma cells were treated with **DPP-2, DPP-7** or **DPP-9A**. The methods are same to those for confocal imaging.

2.11. Breast cancer cell culture, implantation and in vivo imaging

Mouse mammary gland tumor cell line 4T1 was obtained from the ATCC (Manassas, VA). 4T1-luc2 is a luciferase expressing cell line, which was stably transfected with firefly luciferase gene (luc2). Cells were grown in high glucose RPMI 1640 medium (ATCC). Media was supplemented with 10% fetal bovine serum (Hyclone, UT) without antibiotics. All procedures for animal care and tumor cell implantation followed the approved animal protocols and guidelines of the

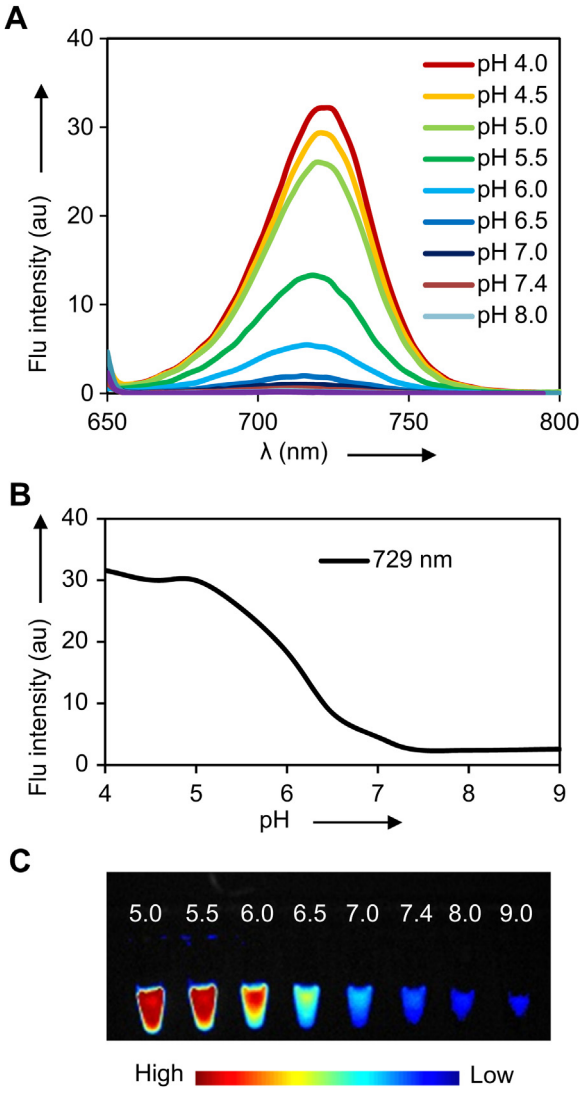

Fig. 2. Characterization of pH-dependent electron donor-acceptor fluorescence system **9A**. (A) Fluorescence spectra of fluorophore-dopamine conjugate **9A** in different PBS. Spectra were collected on a Perkin–Elmer LS-55 spectrofluorometer with excitation 640 nm. (B) Plot of fluorescence emission at 729 nm versus pH. (C) Fluorescence output of **9A** in different PBS was imaged and registered on a Cri imaging system.

Institutional Animal Care and Use Committee at Caliper Life Sciences. Prior to implantation, all tumor cells tested negative for the presence of mycoplasma and mouse pathogens. The orthotopic implantation of 4T1-luc2-1A4 cells into mammary fat pads of nu/nu or Balb/c mice was performed while animals were under isoflurane anesthesia. Prior to the in vivo imaging, the mice were anesthetized with isoflurane. D-luciferin solution was then injected intraperitoneally (150 mg/kg). The mice were imaged using an IVIS Spectrum. Bioluminescent signals were quantified using Living Image 3.0 (Caliper Life Sciences, Alameda, CA). Then animals with similar sized tumor were randomly divided into two groups. One group received **DPP-2** intravenously with the dose of 20 μg fluorophore units per mouse, the other group **DPP-9A**. Fluorescent imaging was performed pre-injection, 15 min, 1 h, 3 h, 6 h, 24 h and 72 h post-injection.

2.12. Glioma cell implantation and in vivo imaging

U87 MG-luc2 is a luciferase expressing cell line which was stably transfected with firefly luciferase gene (luc2). U87-luc2 orthotopic glioma model, using the human U87-luc2 glioma cell line, was created in nude mice. About 4-week old male Balb/c nude mice of 16–18 g body weight were provided by Caliper Life Sciences and maintained under standard housing conditions. All procedures for animal care and tumor cell implantation followed the approved animal protocols and guidelines of the Institutional Animal Care and Use Committee at Caliper Life Sciences. Briefly, 5.0×10^4 U87 cells in 5 μL Hank's balanced salt solution (HBSS) were slowly (over 2 min) implanted 3 mm deep into the right caudatoputamen. After implantation of

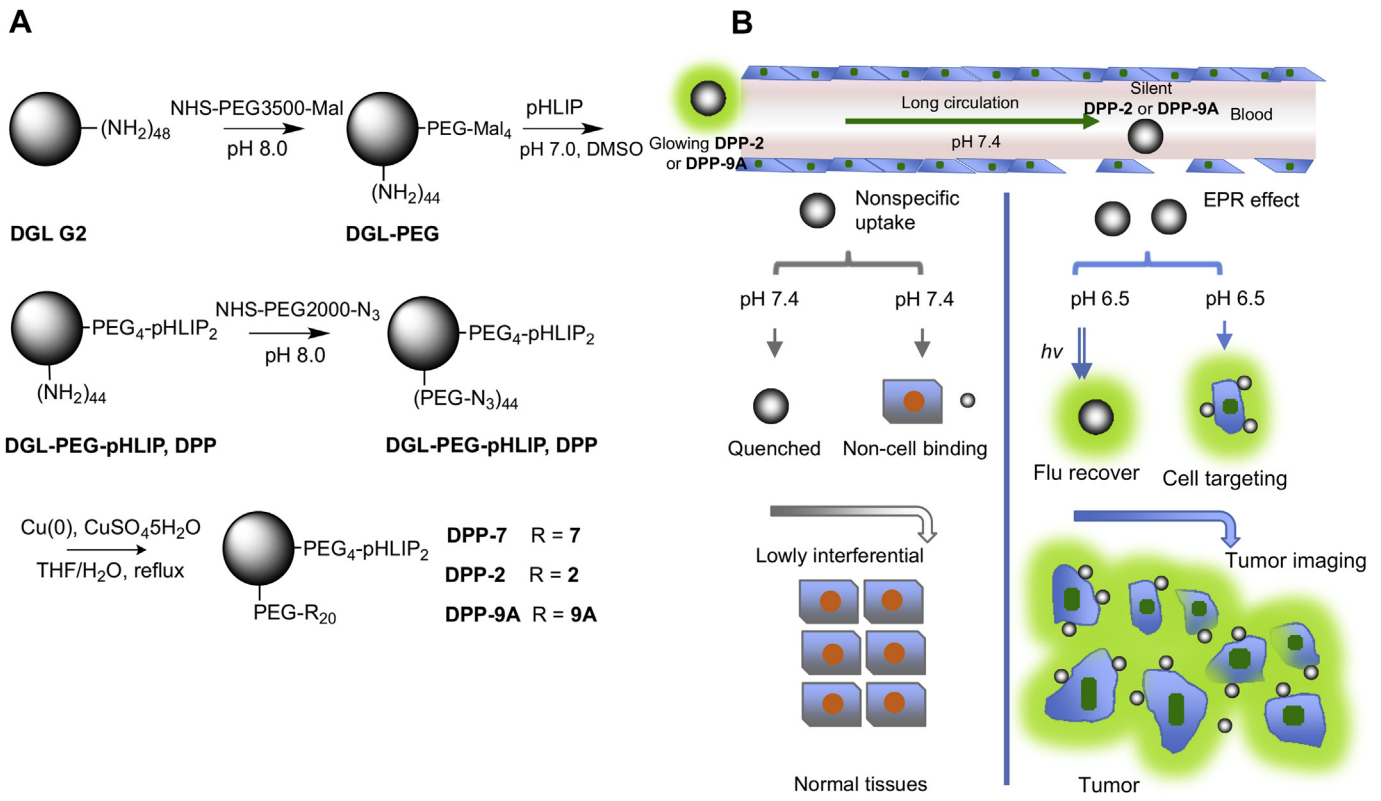

Fig. 3. Tumor cell membrane-targeting pH-dependent electron donor-acceptor systems for low interferential tumor imaging. (A) The synthetic procedure for tumor cell membrane-targeting imaging systems. (B) Improved circulation time can make sufficient contact with alkalescent physiological environment for complete quenching of fluorescence. pHLIP-induced membrane insertion and zero potential can specially transfer silent fluorophore to tumor extracellular environment and make **DPP-2** or **DPP-9A** stay at cell membrane. Tumor-accumulated fluorophore can be activated by acidic pH.

the cells, the needle was left in place for 5 min, and then slowly withdrawn from the brain, and the skin incision closed. Twenty days after surgery, glioma-bearing mice were employed for in vivo bioluminescence imaging. Then animals were randomly divided into two groups. One group received **DPP-2** intravenously with the dose of 20 μg fluorophore per mouse, the other group **DPP-9A**. Fluorescent imaging was performed 30 min, 1 h, 2 h, and 4 h post-injection.

3. Results

3.1. Synthesis and characterization of fluorophore-dopamine conjugate *9A*

The synthetic route commenced with an addition of chloracetyl chloride to dopamine, which gave activated dopamine **4** (Supplementary Information, Fig. S1). Subsequent hydroxyl protection was achieved by addition of chloromethyl methyl ether. Then this activated and hydroxyl-protected dopamine **5** was reacted with the monophenol of **2** to obtain **9A** (MS and NMR information in Methods and Supplementary Information, Fig. S2). The dual-alkyne-substituted boron-chelated tetraarylazadipyrromethene **7** was used as a control and synthesized as previously described [23].

The fluorescence spectral features of **9A** in different PBS are shown in Fig. 2. In contrast to **7** (Supplementary Information, Fig. S3), the spectral properties of **9A** displayed a striking response across the physiological pH range (Fig. 2). A sigmoidal plot of pH versus fluorescence intensity predicted an apparent pKa of 6.17 (Fig. 2B). Fluorescence output gradually decreased as pH increased. The excited state response of **9A** at the λ_{max} of 729 nm in aqueous solutions showed a greater than 4-fold fluorescence intensity differential between pH 6.5 and 7.4 with virtually complete suppression of fluorescence signal at pH 8 (Fig. 2B). Similar quenching trend was also observed by Cri imaging system (Fig. 2C). Our results indicated that the fluorescence output of **9A** is dependent on the pH change. Therefore, the underlying quenching mechanism may be the pH-dependent electron transfer. Similar phenomenon was also found when investigating the fluorescence spectral features of **2** (Supplementary Information, Fig. S3). A sigmoidal plot of pH versus fluorescence intensity predicted an apparent pKa of 5.40 (Supplementary Information, Fig. S3).

Next, we evaluated the feasibility of imaging tumor cells by free **2** and **9A**. Considering their hydrophobicity, free fluorophores were encapsulated in micelle for treatment. Free fluorophores **2** and **9A** enter cells both in pH 7.4 and in pH 6.5 (Supplementary Information, Fig. S4). The infrared fluorescence was shown in the whole of the cells. This indicated that free fluorophores are internalized by passive diffusion. The yellow signal suggested that a portion of fluorophore is inside endosome/lysosome. There is no significant difference of fluorescence of cells in different pH. Intracellular acidity would result to high interferential signal. Hence, free fluorophores cannot be directly used for in vivo imaging.

3.2. Synthesis and characterization of tumor cell membrane-targeting imaging systems

The tumor cell membrane-targeting imaging systems are synthesized as previously described with minor modification (Fig. 3A) [34]. First, pHLIP was conjugated to the surface of the DGL *via* a-Malemidyl-u-N-hydroxysuccinimidyl polyethylene glycol (NHS-PEG-MAL, MW 3500) to obtain DGL-PEG-pHLIP (**DPP**). Then **DPP** was reacted with excess a-azide-u-N-hydroxysuccinimidyl polyethylene glycol (NHS-PEG-N_3, MW 2000) for conjugating the

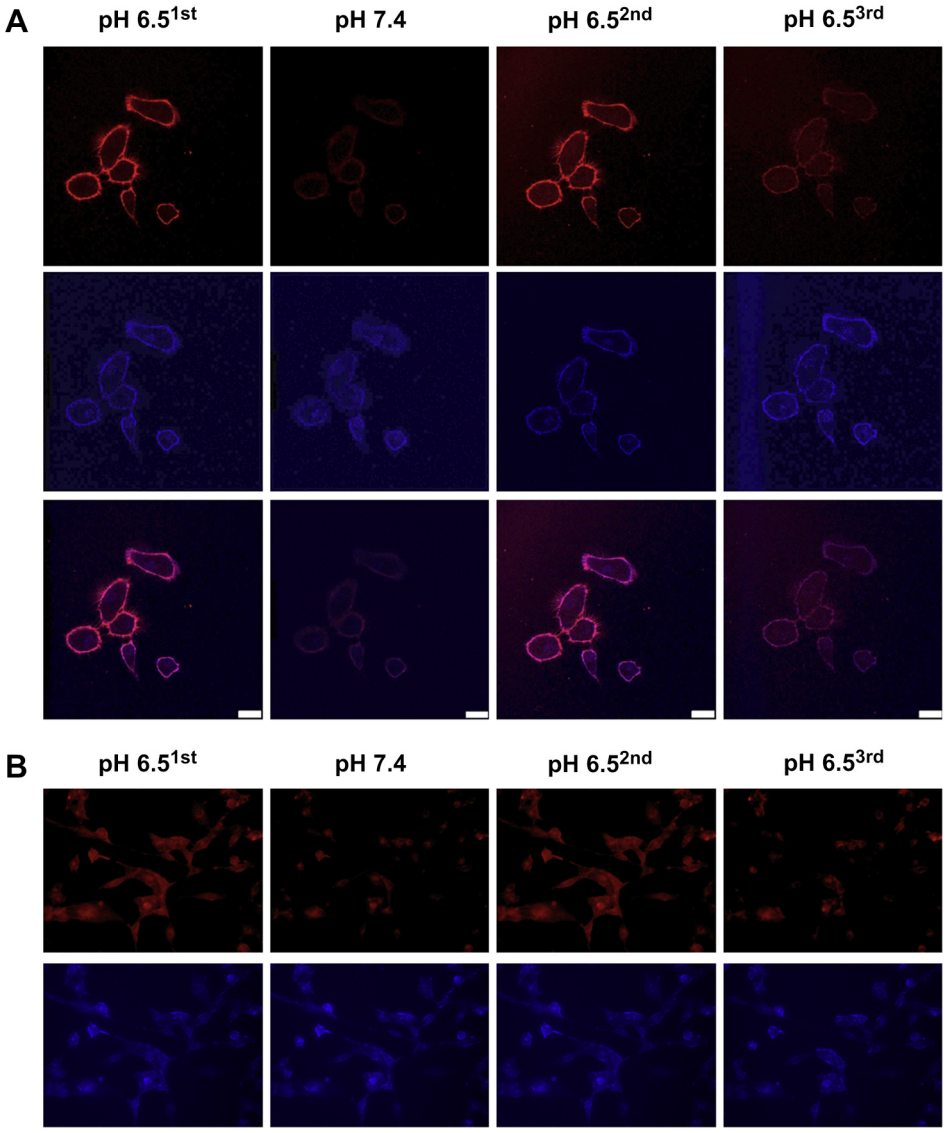

Fig. 4. In vitro tumor extracellular pH-sensing by tumor cell membrane-targeting fluorescence system **DPP-9A**, which demonstrated its tumor cell membrane targeting and pH-sensitive fluorescence. The fluorescence and cellular location of **DPP-9A** were examined in Bel-7402 cancer cells (A) and U87 glioma cells (B) in different conditions. pH 6.5^{1st}, 5 min incubation in PBS 6.5; pH 7.4, medium 6.5 was carefully replaced by medium 7.4; pH 6.5^{2nd}, medium 7.4 was replaced by medium 6.5; pH 6.5^{3rd}, cells were washed thoroughly with PBS 7.4 and medium was replaced by medium 6.5 (v). Blue: Cell membrane. Red: **DPP-9A**. Purple: Cell membrane marker colocalized with **DPP-9A**. (For interpretation of the references to color in this figure legend, the reader is referred to the web version of this article.)

alkyne group of **9A**. Excess PEG can enhance the hydrophilicity and minimize the positive potential to limit intracellular uptake and prolong circulation time. The water solubility of **DPP-2** and **DPP-9A** could reach 200 μg/ml. The in vivo pharmacokinetic behavior of the tumor cell membrane-targeting imaging systems is predicted in Fig. 3B. Improved circulation time can make sufficient contact with alkalescent physiological environment for complete quenching of fluorescence and low interferential signal. pHLIP-induced membrane insertion and zero potential can specially transfer quenched fluorophore to tumor extracellular environment and make silent imaging systems stay at cell membrane. These tumor-accumulated imaging systems can be activated by acidic pH.

We monitored the emission spectra of **DPP-2** and **DPP-9A** (Supplementary Information, Fig. S5). **DPP-2** and **DPP-9A** showed fluorescence features similar to those of **2** and **9A**. The spectral properties of **DPP-2** and **DPP-9A** displayed striking responses across the physiological pH range. Fluorescence output gradually decreased as pH increased. Sigmoidal plots of pH versus fluorescence intensity predicted apparent pKa of 5.45 and 6.03. The excited state response of **DPP-2** and **DPP-9A** at the λ_{max} of 729 nm in aqueous solutions showed greater than 4-fold fluorescence intensity differentials between pH 6.5 and 7.4 with virtually complete suppression of fluorescence signal at pH 8.

3.3. In vitro cell imaging

We evaluated whether tumor cell membrane-targeting pH-dependent electron donor-acceptor fluorescence systems **DPP-2** and **DPP-9A** could monitor extracellular pH difference between normal tissue and tumor. Mediums with different pH were utilized to imitate the in vivo extracellular environments. All fluorescence imaging systems **DPP-7**, **DPP-2** and **DPP-9A** targeted and stayed at the cell membrane in pH 6.5 medium (see pH 6.5^{1st} in Figs. 4 and 5 and Supplementary Information, Fig. S6). Then medium was switched to pH 7.4. The intensity of **DPP-7** at cell membrane didn't change (pH 7.4 in Supplementary Information, Fig. S6). This

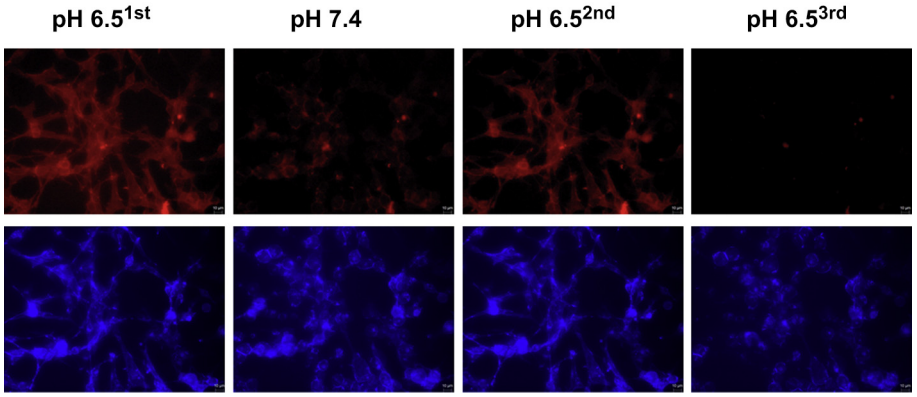

Fig. 5. In vitro U87 glioma extracellular pH-sensing by tumor cell membrane-targeting pH-dependent fluorescence system **DPP-2**, which showed tumor cell membrane targeting and pH-sensitive fluorescence. The fluorescence and cellular location of **DPP-2** were examined in different conditions. pH 6.5^{1st}, 5 min incubation in PBS 6.5; pH 7.4, medium 6.5 was carefully replaced by medium 7.4; pH 6.5^{2nd}, medium 7.4 was replaced by medium 6.5; pH 6.5^{3rd}, cells were washed thoroughly with PBS 7.4 and medium was replaced by medium 6.5 (v). Blue: Cell membrane. Red: **DPP-2**. Purple: Cell membrane marker colocalized with **DPP-2**. (For interpretation of the references to color in this figure legend, the reader is referred to the web version of this article.)

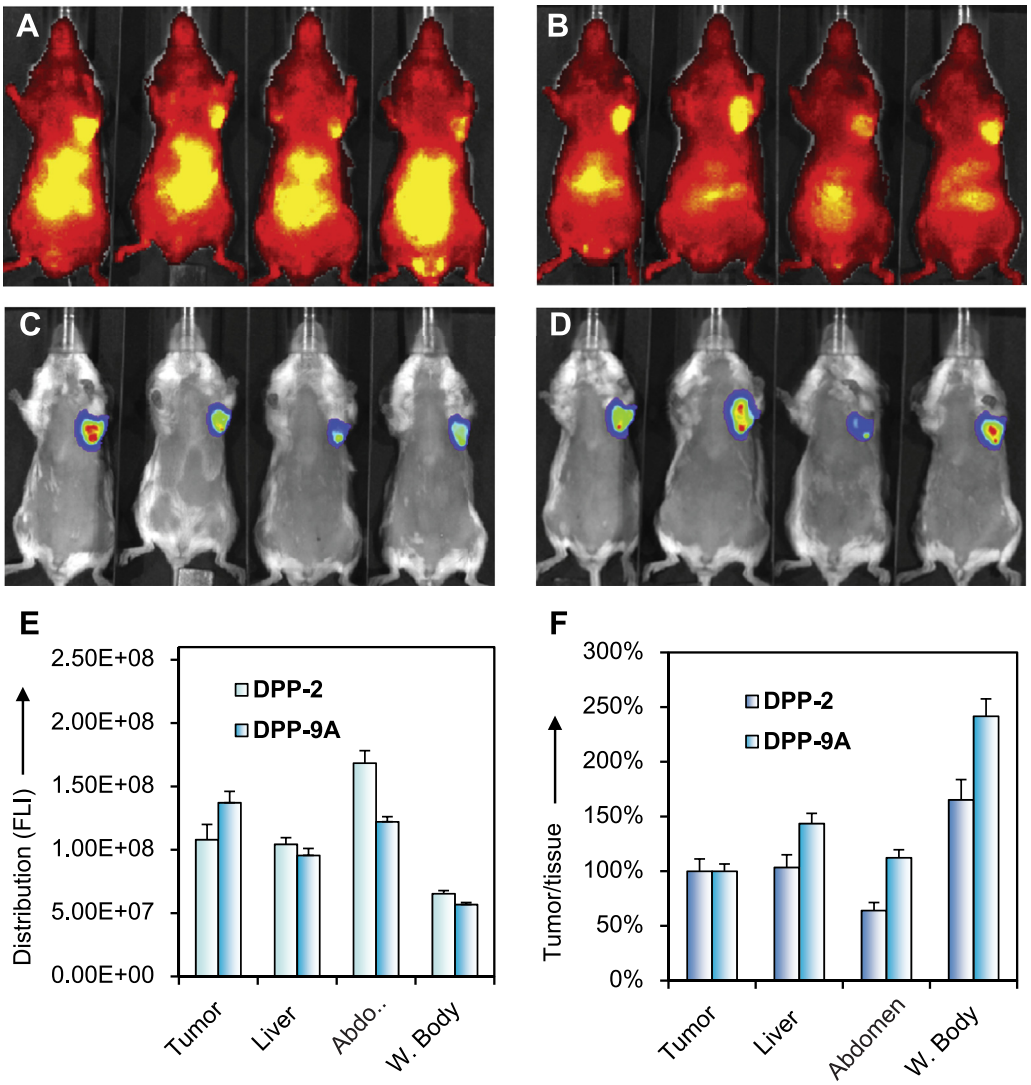

Fig. 6. In vivo breast cancer imaging by tumor cell membrane-targeting pH-dependent electron donor-acceptor fluorescence systems. In vivo imaging of mice administrated with **DPP-2** (A) or **DPP-9A** (B). Images were taken 24 h after treatment. (C and D) Bioluminescence imaging of the locations of breast cancer at 24 h. (E) The signal in different tissues was quantified. (F) Tumor/background ratio was calculated.

demonstrated the pH-insensitivity of **DPP-7**. While the fluorescence intensity of **DPP-2** and **DPP-9A** at cell membrane dramatically decreased (pH 7.4 in Figs. 4 and 5), indicating that pH change silenced glowing **DPP-2** and **DPP-9A**. This demonstrated the pH-sensitivity of **DPP-2** and **DPP-9A**. The second change of medium from pH 7.4 to pH 6.5 showed no change of the signal of **DPP-7** (see pH 6.5^{2nd} in Supplementary Information, Fig. S6). However, the signal of **DPP-2** and **DPP-9A** was recovered (pH 6.5^{2nd} in Figs. 4 and 5), suggesting acidic pH could make silent **DPP-2** glowing. The second medium indirectly proved the insensitivity of **DPP-7** and pH-sensitivity of **DPP-2** and **DPP-9A**. Finally, after cells were washed thoroughly with PBS 7.4, the signal in pH 6.5 at cell membrane treated with all imaging systems dramatically decreased (see pH 6.5^{3rd} in Figs. 4 and 5 and Supplementary Information, Fig. S6). The vigorous washes by pH 7.4 decreased the fluorescence signal at cell membrane due to the reverse of membrane insertion of pHLIP.

3.4. *In vivo low interferential tumor-imaging*

Inspired by the exciting in vitro imaging results, we evaluated the feasibility of low interferential imaging breast cancer in vivo (Fig. 6). We investigated the fluorescence imaging of breast cancer in different time points (Supplementary Information, Figs. S7 and S8). The intensity of signal in both normal tissues and tumor gradually increased till about 24 h. Breast cancer cells can be clearly found by expressed luciferase. In 24 h, the fluorescence signal of **DPP-2** and **DPP-9A** overlapped with the luminescence signal of breast cancer cells. Both **DPP-2** and **DPP-9A** could specially diagnose the orthotropic breast cancers. There is no significant difference between **DPP-2** and **DPP-9A**. There is very low interferential signal in either treated mice. The tumor/non-specific signal ratios were greater than one for both **DPP-2** and **DPP-9A**. Due to the different tumor characteristics in CNS and periphery, we also assessed the feasibility of imaging brain glioma. Both **DPP-2** and **DPP-9A** can specially image the tumor (Fig. 7).

4. Discussion

In this study we have developed low interferential tumor-imaging using environment-targeting pH-dependent electron donor-acceptor fluorescence systems. We have designed and synthesized a pH-dependent activatable near-infrared fluorophore **9A** based on the electron transfer. Environment-targeting electron donor-

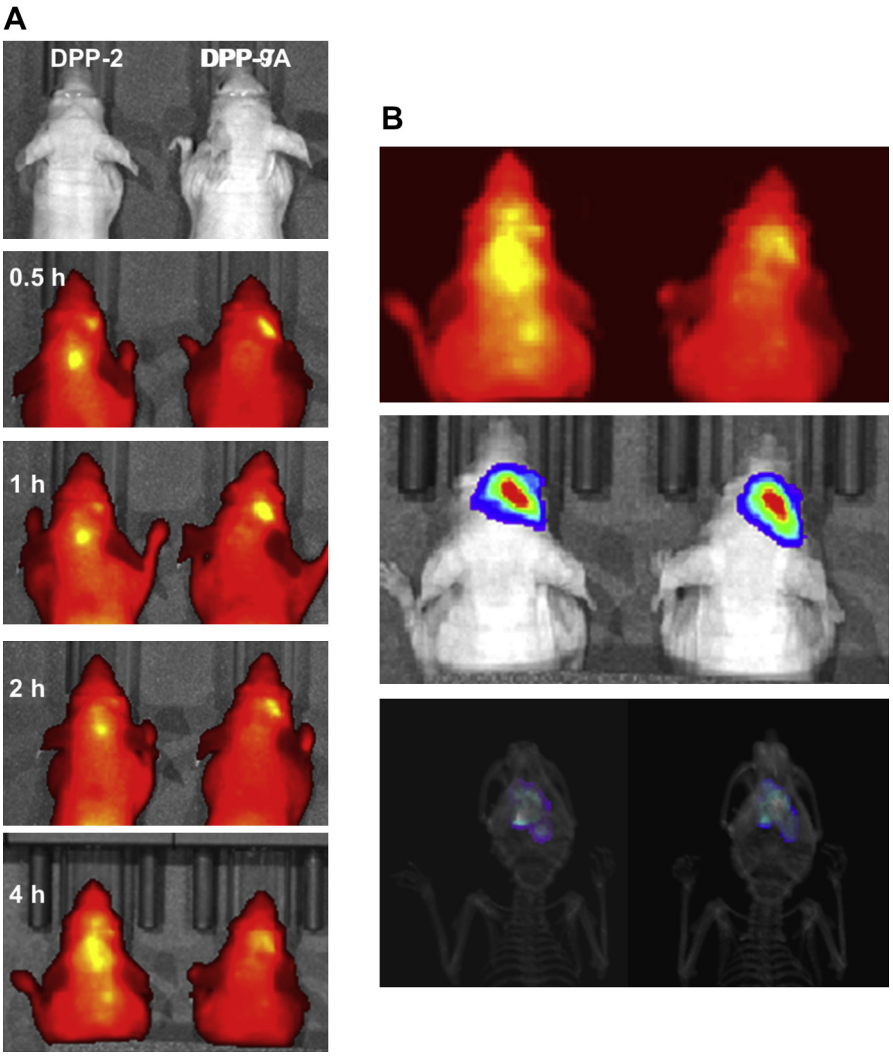

Fig. 7. In vivo brain glioma imaging by tumor cell membrane-targeting pH-dependent electron donor-acceptor fluorescence systems. (A) The fluorescence signal in glioma-bearing brain was registered for a continuous period of time after treatment. (B) The fluorescence image, bioluminescence image and x-ray image at 4 h (to show the glioma location) showed that both **DPP-2** and **DPP-9A** could specifically image the glioma. Left mice, **DPP-2**; right mice, **DPP-9A**.

acceptor fluorescence systems (**DPP-2** and **DPP-9A**) based on tumor extracellular environment targeting carrier **DPP** are highly specific for representative tumors including breast tumor and brain tumor.

This study illustrates the considerable utility of electron transfer for designing the 'activatable' fluorophore. Currently most tumor targeting imaging systems show strong background signal in healthy tissues. Although many activatable fluorescence probes have been developed, the background signal still cannot be completely turned off. The conjugate of fluorophore **2** with single-wall carbon nanotube functioning as an electron acceptor has been investigated [35]. Electron transfer from fluorophore to the electron acceptor can totally quench the fluorescence of the fluorophore. The fluorescence intensity change of fluorophore **2** and **9A** is dependent on the pH change. The tumor extracellular acidosis can activate the fluorescence intensity of fluorophore **2** and **9A**.

Because pH difference between tumor and normal tissues only exists in extracellular environments and free fluorophores could enter both normal cells and tumor cells (Supplementary Information, Fig. S4), tumor extracellular environment targeting needs to be considered for delivery of **2** and **9A**. Hence, efficient delivery systems that could stay in the tumor extracellular region are urgently needed for delivering the activatable fluorophores. The tumor extracellular environment targeting by pHLIP-mediated membrane insertion would increase the retention of the system in tumor extracellular regions. There exist several endocytic mechanisms, including (1) receptor-mediated endocytosis, (2) adsorptive endocytosis, such as electrostatic interactions [36], and (3) macro pinocytosis [37]. In this study, the endocytic mechanisms were turned off for limiting the intracellular uptake of the imaging systems. The strategy is to modify all surface amino groups on DGLs by PEG to enhance the hydrophilicity and minimize the positive potential. According to literature, at pH 7.4, pHLIP doesn't insert the cell membrane but only bind with the cells. The reason for the fluorescence intensity decrease of **DPP-7**, **DPP-2** and **DPP-9A** treated cells after thoroughly PBS 7.4 wash (see pH 6.5^{3rd} in Figs. 4 and 5 and Supplementary Information, Fig. S6) may be the detachment of **DPP-7** from the cell membrane. Hydrophilicity, zero zeta potential and blood flow (imitated by washes) may contribute to the detachment of **DPP-7**, **DPP-2** and **DPP-9A**. Importantly, the difference of signal intensity for tumor extracellular environments (pH 6.5) and physiological environment (pH 7.4) only results from the tumor targeting effect of **DPP-7**. However, for **DPP-2** and **DPP-9A**, the difference of intensity between tumor extracellular environments and physiological environment includes the contribution from the tumor targeting effect and the pH-sensitive fluorescence intensity.

Both **DPP-2** and **DPP-9A** showed lower signal intensity in liver and abdomen in breast cancer-bearing mice (Fig. 6). The lower intensity in these normal tissues may result from the tumor extracellular environment targeting and pH-responsive fluorescence emission. The fluorescence imaging data in different time points demonstrated the long circulating effect (Supplementary Information, Figs. S7 and S8). **DPP-2** and **DPP-9A** are present in bloodstream for a long period of time, which makes glowing **DPP-2** and **DPP-9A** silent. Silent **DPP-2** and **DPP-9A** gradually enter tumor extracellular environment and become bright. The results of brain cancer imaging are consistent with that of detection of breast cancer diagnosis. Subcutaneous tumors have a pore cut-off size ranging from 200 nm to 1.2 μm, which is dramatically reduced when the tumor is grown in the cranial microenvironment [38]. Glioma exhibited a characteristic pore cut-off size ranging from 7 nm to 100 nm [38]. Therefore, **DPP-2** and **DPP-9A** with the size at ~10 nm have great superiority in targeting and imaging gloom.

5. Conclusions

We demonstrated the utility of pH-dependent electron transfer as signal control switch for regulating the fluorescence intensity. We provide a facile method for the synthesis of dopamine-attached fluorophore **9A**. Owing to the many chemically functional amine groups present within DGLs, high fluorophore loading (**2** and **9A**) can be achieved by simple and efficient NHS-PEG-N_3 conjugation. Furthermore, we demonstrate the utility of **DPP-2** and **DPP-9A** as optical imaging contrast agents for the in vitro and in vivo detection of tumor cells. Therefore, we believe that **DPP-2** and **DPP-9A** described herein provide a powerful new platform for the early detection of disease. Of course, before any new organic dye-based contrast can be extended to the clinic, their toxicological profile must be carefully evaluated. This information includes cytotoxicity, tissue toxicity, in vivo toxicity, and mutagenicity. This point is particularly relevant for organic dye-labeled systems, which generally exhibit longer circulation and residence times compared with free organic dye. As a consequence, future work will be aimed at developing biodegradable dendrimers and/or crosslinkers that can be eliminated from the body in a reasonable period of time after carrying out their diagnostic function. Ultimately, the most effective and appropriate probes for use in patients will be determined by their fluorescent characteristics and the safety of the conjugates.

Acknowledgment

This work was supported by the grant from National Basic Research Program of China (973 Program, 2013CB932500), National Natural Science Foundation of China (81172993), and Program for New Century Excellent Talents in University. Supplementary Information is available online from Wiley InterScience or from the author.

Appendix A. Supplementary data

Supplementary data related to this article can be found at http://dx.doi.org/10.1016/j.biomaterials.2013.12.020.

References

[1] Rudin M, Weissleder R. Molecular imaging in drug discovery and development. Nat Rev Drug Discov 2003;2:123–31.
[2] Jiang L, Zhou Q, Mu K, Xie H, Zhu Y, Zhu W, et al. pH/temperature sensitive magnetic nanogels conjugated with Cy5.5-labled lactoferrin for MR and fluorescence imaging of glioma in rats. Biomaterials 2013;34(30):7418–28.
[3] Liu Y, Ai K, Yuan Q, Lu L. Fluorescence-enhanced gadolinium-doped zinc oxide quantum dots for magnetic resonance and fluorescence imaging. Biomaterials 2011;32(4):1185–92.
[4] Qian J, Jiang L, Cai F, Wang D, He S. Fluorescence-surface enhanced Raman scattering co-functionalized gold nanorods as near-infrared probes for purely optical in vivo imaging. Biomaterials 2011;32(6):1601–10.
[5] Huang X, Zhang F, Lee S, Swierczewska M, Kiesewetter DO, Lang L, et al. Long-term multimodal imaging of tumor draining sentinel lymph nodes using mesoporous silica-based nanoprobes. Biomaterials 2012;33(17):4370–8.
[6] Lim E-K, Yang J, Dinney CP, Suh J-S, Huh Y-M, Haam S. Self-assembled fluorescent magnetic nanoprobes for multimode-biomedical imaging. Biomaterials 2010;31(35):9310–9.
[7] Xing H, Bu W, Zhang S, Zheng X, Li M, Chen F, et al. Multifunctional nanoprobes for upconversion fluorescence, MR and CT trimodal imaging. Biomaterials 2012;33(4):1079–89.
[8] Kobayashi H, Ogawa M, Alford R, Choyke PL, Urano Y. New strategies for fluorescent probe design in medical diagnostic imaging. Chem Rev 2010;110(5):2620–40.
[9] Hama Y, Urano Y, Koyama Y, Kamiya M, Bernardo M, Paik RS, et al. A target cell-specific activatable fluorescence probe for in vivo molecular imaging of cancer based on a self-quenched avidin-rhodamine conjugate. Cancer Res 2007;67(6):2791–9.
[10] Urano Y, Asanuma D, Hama Y, Koyama Y, Barrett T, Kamiya M, et al. Selective molecular imaging of viable cancer cells with pH-activatable fluorescence probes. Nat Med 2009;15(1):104–9.

[11] Kobayashi H, Choyke PL. Target-cancer-cell-specific activatable fluorescence imaging probes: rational design and in vivo applications. Acc Chem Res 2011;44(2):83–90.
[12] Hynes NE, Lane HA. ERBB receptors and cancer: the complexity of targeted inhibitors. Nat Rev Cancer 2005;5(5):341–54.
[13] Xu Z, Gu W, Huang J, Sui H, Zhou Z, Yang Y, et al. In vitro and in vivo evaluation of actively targetable nanoparticles for paclitaxel delivery. Int J Pharm 2005;288(2):361–8.
[14] Wagner E, Zenke M, Cotten M, Beug H, Birnstiel ML. Transferrin-polycation conjugates as carriers for DNA uptake into cells. Proc Natl Acad Sci U S A 1990;87(9):3410–4.
[15] Schiffer E, Housset C, Cacheux W, Wendum D, Desbois-Mouthon C, Rey C, et al. Gefitinib, an EGFR inhibitor, prevents hepatocellular carcinoma development in the rat liver with cirrhosis. Hepatology 2005;41(2):307–14.
[16] Roth P, Hammer C, Piguet AC, Ledermann M, Dufour JF, Waelti E. Effects on hepatocellular carcinoma of doxorubicin-loaded immunoliposomes designed to target the VEGFR-2. J Drug Target 2007;15(9):623–31.
[17] Rao J, Dragulescu-Andrasi A, Yao H. Fluorescence imaging in vivo: recent advances. Curr Opin Biotechnol 2007;18(1):17–25.
[18] Blum G, Mullins SR, Keren K, Fonovič M, Jedeszko C, Rice MJ, et al. Dynamic imaging of protease activity with fluorescently quenched activity-based probes. Nat Chem Biol 2005;1(4):203–9.
[19] Fonović M, Bogyo M. Activity based probes for proteases: applications to biomarker discovery, molecular imaging and drug screening. Curr Pharm Des 2007;13(3):253–61.
[20] Gorman A, Killoran J, O'Shea C, Kenna T, Gallagher WM, O'Shea DF. In vitro demonstration of the heavy-atom effect for photodynamic therapy. J Am Chem Soc 2004;126(34):10619–31.
[21] Michael J, McDonnell SO, Killoran J, O'Shea DF. A modular synthesis of unsymmetrical tetraarylazadipyrromethenes. J Org Chem 2005;70(14):5571–8.
[22] Tasior M, O'Shea DF. BF2-Chelated tetraarylazadipyrromethenes as NIR Fluorochromes. Bioconjug Chem 2010;21(7):1130–3.
[23] Murtagh J, Frimannsson DO, O'Shea DF. Azide conjugatable and pH responsive near-infrared fluorescent imaging probes. Org Lett 2009;11(23):5386–9.
[24] Clarke SJ, Hollmann CA, Zhang Z, Suffern D, Bradforth SE, Dimitrijevic NM, et al. Photophysics of dopamine-modified quantum dots and effects on biological systems. Nat Mater 2006;5(5):409–17.
[25] Cooper DR, Suffern D, Carlini L, Clarke SJ, Parbhoo R, Bradforth SE, et al. Photoenhancement of lifetimes in CdSe/ZnS and CdTe quantum dot-dopamine conjugates. Phys Chem Chem Phys 2009;11(21):4298–310.
[26] Medintz IL, Stewart MH, Trammell SA, Susumu K, Delehanty JB, Mei BC, et al. Quantum-dot/dopamine bioconjugates function as redox coupled assemblies for in vitro and intracellular pH sensing. Nat Mater 2010;9(8):676–84.
[27] Gerweck LE, Seetharaman K. Cellular pH gradient in tumor versus normal tissue: potential exploitation for the treatment of cancer. Cancer Res 1996;56(6):1194–8.
[28] Makovitzki A, Fink A, Shai Y. Suppression of human solid tumor growth in mice by intratumor and systemic inoculation of histidine-rich and pH-dependent host defense-like lytic peptides. Cancer Res 2009;69(8):3458–63.
[29] Zhang X, Lin Y, Gillies RJ. Tumor pH and its measurement. J Nucl Med 2010;51(8):1167–70.
[30] Gillies R, Liu Z, Bhujwalla Z. 31P-MRS measurements of extracellular pH of tumors using 3-aminopropylphosphonate. Am J Phys 1994;267(1 Pt 1):C195–203.
[31] Raghunand N, He X, Van Sluis R, Mahoney B, Baggett B, Taylor C, et al. Enhancement of chemotherapy by manipulation of tumour pH. Br J Cancer 1999;80(7):1005–11.
[32] Hunt JF, Rath P, Rothschild KJ, Engelman DM. Spontaneous, pH-dependent membrane insertion of a transbilayer alpha-helix. Biochemistry 1997;36(49):15177–92.
[33] Chauhan VP, Popović Z, Chen O, Cui J, Fukumura D, Bawendi MG, et al. Fluorescent nanorods and nanospheres for real-time in vivo probing of nanoparticle shape-dependent tumor penetration. Angew Chem Int Ed Engl 2011;50(48):11417–20.
[34] Han L, Ma H, Guo Y, Kuang Y, He X, Jiang C. pH-controlled delivery of nanoparticles into tumor cells. Adv Healthc Mater 2013;2:1435–9.
[35] Flavin K, Lawrence K, Bartelmess J, Tasior M, Navio C, Bittencourt C, et al. Synthesis and characterization of boron azadipyrromethene single-wall carbon nanotube electron donor-acceptor conjugates. ACS Nano 2011;5(2):1198–206.
[36] Smith MW, Gumbleton M. Endocytosis at the blood-brain barrier: from basic understanding to drug delivery strategies. J Drug Target 2006;14(4):191–214.
[37] Walsh M, Tangney M, O'Neill M, Larkin J, Soden D, McKenna S, et al. Evaluation of cellular uptake and gene transfer efficiency of pegylated poly-L-lysine compacted DNA: implications for cancer gene therapy. Mol Pharmacol 2006;3(6):644–53.
[38] Hobbs SK, Monsky WL, Yuan F, Roberts WG, Griffith L, Torchilin VP, et al. Regulation of transport pathways in tumor vessels: role of tumor type and microenvironment. Proc Natl Acad Sci U S A 1998;95(8):4607–12.